RSC Advances

PAPER

View Article Online
View Journal | View Issue

Open Access Article. Published on 16 March 2018. Downloaded on 5/9/2026 5:12:19 PM.
This article is licensed under a Creative Commons Attribution-NonCommercial 3.0 Unported Licence.

Check for updates

Cite this: *RSC Adv.*, 2018, **8**, 10756

Solvent-tuned charge-transfer properties of chiral Pt(II) complex and $TCNQ^{\bullet-}$ anion adducts†

Xiao-Peng Zhang,* Li-Li Wang, Da-Shuai Zhang, Xiao-Wei Qi, Zai-Feng Shi* and Qiang Lin

Received 11th February 2018
Accepted 4th March 2018

DOI: 10.1039/c8ra01330f

rsc.li/rsc-advances

A new pair of adducts comprising one chiral Pt(II) complex cation, $[Pt((-)\text{-}L_1)(Dmpi)]^+$ ((−)-**1**) or $[Pt((+)\text{-}L_1)(Dmpi)]^+$ ((+)-**1**) [(−)-L_1 = (−)-4,5-pinene-6′-phenyl-2,2′-bipyridine, (+)-L_1 = (+)-4,5-pinene-6′-phenyl-2,2′-bipyridine, Dmpi = 2,6-dimethylphenylisocyanide], together with one $TCNQ^{\bullet-}$ anion have been obtained, and the structures have been confirmed *via* single-crystal X-ray crystallography and infrared (IR) spectroscopy. The chiral Pt(II) cation and $TCNQ^{\bullet-}$ anion are dissociated in MeOH solution, while charge transfer adducts are formed in H_2O solution, leading to perturbation of the electronic structure and alteration of the chiral environment, as evidenced by the differences in the UV-vis absorption and electronic circular dichroism spectra. The solvent-tuned charge-transfer properties also have been validated through emission and resonance light scattering spectra. The interesting findings may have potential applications in the development of black absorbers and wide band gap semiconductors.

1. Introduction

Square-planar platinum(II) complexes have been the subject of intensive research due to their great potential in the exploration of novel molecular materials and advanced electronic devices.[1–6] Under special environmental stimuli, square-planar molecules are expected to form supramolecular aggregates through extended *intermolecular interactions, *e.g.* Pt···Pt and π–π contacts.[7–14] In most cases, variances in color, luminescence, viscosity and morphology accompany stimuli–responsive processes, with aggregates showing intriguing solvatochromism,[15,16] vapochromism,[17–19] mechanochromism[20–22] and thermochromism[23]. With regards to solvatochromism, the assembled structures can be tuned through the solvent composition, and remarkable changes in UV-vis absorption and emission characteristics can be induced through the variation of solvents.[24] Additionally, helical assemblies of Pt(II) complexes can be formed in solution with the introduction of optically pure groups, correspondingly leading to interesting on–off switching of chiral signals.[25–30] It is suggested that these above-mentioned stimuli-induced switches can be harnessed to develop versatile sensors to detect subtle environmental changes.[31–34]

7,7,8,8-Tetracyanoquinodimethane (TCNQ) has been widely investigated as a good electron acceptor due to its high electron affinity. As a classical example, TCNQ can form a charge transfer (CT) complex with an electron acceptor, showing unique conducting and magnetic properties with high charge density.[35–37] More importantly, the open shell electron radical $TCNQ^{\bullet-}$ anion can be readily formed through one electron reduction, and versatile CT complexes can be assembled *via* the combination of $TCNQ^{\bullet-}$ with a large number of cations (metal ions, organic cations and organometallic complexes).[38–42] Compared to TCNQ, these CT materials based on $TCNQ^{\bullet-}$ are endowed with higher conductivity, even superconductivity, due to a low band gap, offering promise for the development of the semiconductor industry.[38,39,43] Moreover, ion-, vapor-, mechano-, and photo-induced multi-dimensional switches have been reported, and different conformations, alternating stackings and intermolecular CT capabilities can be modulated under specific stimuli.[44–46]

In general, the $TCNQ^{\bullet-}$ anion interacts with other cations to form CT adducts through π–π and hydrogen-bonding interactions; CT adducts containing Pt(II) complexes and $TCNQ^{\bullet-}$ would be of special interest because effective Pt–π contacts may be found, therefore leading to more interesting spectroscopic, magnetic and conductive properties.[47] Due to intensive charge transfer interactions between Pt(II) complexes and $TCNQ^{\bullet-}$, their adducts exhibit continuous UV-vis-NIR absorptions spanning *ca.* 200–1500 nm, and the lowest energy absorption is a characteristic band from a donor/acceptor charge transfer transition that is absent in the absorption spectra of dissociated molecules of the donor or acceptor.[47] Given their strong absorptions across the visible–NIR region, these adducts can

Key Laboratory of Water Pollution Treatment & Resource Reuse of Hainan Province, College of Chemistry and Chemical Engineering, Hainan Normal University, Haikou 571158, People's Republic of China. E-mail: zxp_inorganic@126.com; zaifengshi_hnnu@sina.com; Tel: +86-898-65889422

† Electronic supplementary information (ESI) available. CCDC 1823177 ((−)-**1**/(+)-**1**-TCNQ). For ESI and crystallographic data in CIF or other electronic format see DOI: 10.1039/c8ra01330f

 This journal is © The Royal Society of Chemistry 2018

Open Access Article. Published on 16 March 2018. Downloaded on 5/9/2026 5:12:19 PM.
This article is licensed under a Creative Commons Attribution-NonCommercial 3.0 Unported Licence.

serve as competitive candidates for black body absorbers, opening up potential applications in wide band gap semiconductors and solar cells.[48]

In previous work, we have investigated vapor-, solvent-, mechano-, redox- and temperature-induced structural and spectroscopic switches involving chiral square-planar Pt(II) complexes.[49–54] Among the Pt(II) complexes reported by us, the cationic complexes $[Pt((-)\text{-}L_1)(Dmpi)]^+$ ((−)-**1**) and $[Pt((+)\text{-}L_1)(Dmpi)]^+$ ((+)-**1**), [(−)-L_1 = (−)-4,5-pinene-6′-phenyl-2,2′-bipyridine, (+)-L_1 = (+)-4,5-pinene-6′-phenyl-2,2′-bipyridine, Dmpi = 2,6-dimethylphenylisocyanide] have good solubility in both MeOH and H_2O solution, and show distinct aggregate behavior in different solvents.[50] In addition, through varying the counteranions, more pronounced mechanochromic luminescence can be induced.[51] In view of the above-mentioned interesting phenomena with respect to the (−)-**1** and (+)-**1** cations, we envisage that replacing the "spectroscopically innocent" Cl^- counterions with the stable organic radical $TCNQ^{\bullet-}$ would give versatile CT behavior in different solvents. Therefore, as an extension of previous work, a pair of chiral CT complexes, (−)-**1**-TCNQ and (+)-**1**-TCNQ, have been facilely prepared (Chart 1), and the structures of the adducts have been confirmed *via* X-ray analysis. Solvent-induced variances in absorption, luminescence and chiral spectra have been thoroughly investigated.

2. Experimental section

2.1 General methods

All reagents were purchased from commercial suppliers and used as received. The IR spectra were recorded using a Thermo Scientific Nicolet 6700 Fourier transform infrared spectrometer as KBr pellets. UV-vis spectra were recorded on a UV-3600 spectrophotometer. The powder XRD patterns were recorded on a Shimadzu XD-3A X-ray diffractometer. Elemental analysis was performed on a Perkin-Elmer 240C analyzer. EPR spectra were obtained using an EMX-10/12 electron paramagnetic resonance spectrometer. Photoluminescence (PL) spectra were recorded using a Hitachi F-4600 PL spectrophotometer (λ_{ex} = 420 nm). The resonance light scattering (RLS) spectra were obtained through synchronously scanning the excitation and emission monochromators (namely, $\Delta\lambda$ = 0.0 nm) of a Hitachi F-4600 fluorescence spectrophotometer over the wavelength region from 300 to 820 nm (using a 10 mm quartz cell for a concentration of 10^{-5} mol L^{-1}). The electronic circular dichroism (ECD) spectra in MeOH and H_2O solutions were recorded on a Jasco J-810 spectropolarimeter (using a 10 mm quartz cell for a concentration of 5×10^{-5} mol L^{-1}).

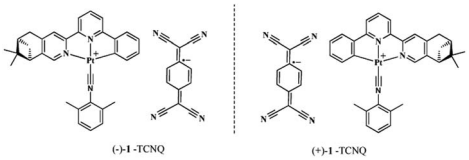

Chart 1 The molecular structures of the CT complexes (−)-**1**-TCNQ and (+)-**1**-TCNQ.

2.2 Synthesis

According to the previous method,[50,51] the cationic complexes (−)-**1** and (+)-**1** were prepared *via* a simple ligand metathesis reaction between the corresponding cyclometalated platinum(II) chloride precursor and 2,6-dimethylphenylisocyanide. The preparation of solid powders of (−)-**1**-TCNQ and (+)-**1**-TCNQ was achieved *via* the slow interfacial diffusion of equal amounts of (−)-**1**/(+)-**1** and LiTCNQ in MeOH or H_2O solution at 278 K. The solution of LiTCNQ was placed at the bottom of a tube, and the corresponding solution of (−)-**1**/(+)-**1** was placed at the top of the tube. The solids were obtained *via* filtration. IR (KBr, cm^{-1}): 716, 733, 749, 766, 815, 823, 835, 985, 1174, 1280, 1324, 1360, 1430, 1470, 1501, 1570, 1603, 2174, 2928, and 3438 (broad). Anal. calcd for $C_{44}H_{34}N_7Pt$ ((−)-**1**-TCNQ): C, 61.75; H, 4.00; N, 11.46%. Found: C, 61.78; H, 4.02; N, 11.45%.

2.3 X-ray structure determination

Single-crystal X-ray diffraction measurements were carried out on a Bruker SMART APEX CCD based on a diffractometer operating at room temperature. Intensities were collected with graphite monochromatized Mo Kα radiation (λ = 0.71073 Å), operating at 50 kV and 30 mA, and using the $\omega/2\theta$ scan mode. Data reduction was made with the Bruker SAINT package.[55] Absorption corrections were performed using the SADABS program.[56] The structures were solved by direct methods and refined based on F^2, *via* full-matrix least-squares, using SHELXL-97 with anisotropic displacement parameters for all non-hydrogen atoms in both structures. Hydrogen atoms bonded to carbon atoms were placed in calculated positions and refined in riding mode, with C–H = 0.93 Å (methane) or 0.96 Å (methyl), and $U_{iso}(H) = 1.2U_{eq}$ ($C_{methane}$) or $U_{iso}(H) = 1.5U_{eq}$ (C_{methyl}). The H_2O hydrogen atoms were located in the difference Fourier maps and refined with an O–H distance restraint [0.85(1) Å] and Uiso(H) = 1.5 Ueq(O). All computations were carried out using the SHELXTL-97 program package.[57] CCDC 1823177 contains the supplementary crystallographic data for this paper.

3. Results and discussion

3.1 Synthesis and characterization

Adduct solids with different morphologies were prepared through slow diffusion at the interface of (−)-**1**/(+)-**1** and LiTCNQ solutions. Deep-green powder (Form-M) is obtained in MeOH, while the solid (Form-H) formed in H_2O (Fig. 1) appears black blue. Despite the difference in color, both adduct solids are non-emissive at room temperature and exhibit similar IR

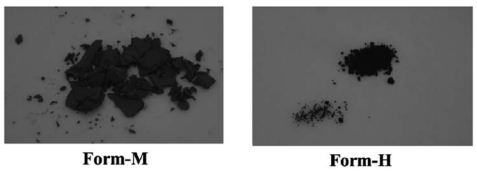

Fig. 1 Photographs of Form-M and Form-H.

Open Access Article. Published on 16 March 2018. Downloaded on 5/9/2026 5:12:19 PM.
This article is licensed under a Creative Commons Attribution-NonCommercial 3.0 Unported Licence.

spectra with strong absorption at 2177 cm^{-1}, ascribed to C≡N stretching vibrations (Fig. S1†), which is the characteristic absorption of the $TCNQ^{\bullet-}$ anion.[38–42,47] Additionally, EPR spectra have been measured, and the *g*-factors of Form-M (g = 2.003) and Form-H (g = 2.004) are almost the same (Fig. S2†), which is attributed to the unpaired electron of the $TCNQ^{\bullet-}$ radical anion.[58]

The UV-vis absorption spectra of the two solid-state species have been studied (Fig. S3†), and both solids show strong absorptions throughout the visible and into the NIR range. In contrast to Form-M, the absorption of Form-H extends to a longer wavelength, and a broad low-energy band centered at *ca.* 1280 nm can be unambiguously observed. It can be speculated that the molecules are packed more closely in Form-H than in Form-M, therefore they induce a stronger donor-to-acceptor charge transfer interaction and result in further absorption into the near-IR region.[47,48] Other than the differences in color and absorption, a distinct difference in the degree of crystallinity is observed between the two solid species (Fig. 2). Form-M reveals intense and narrow peaks, while the XRD pattern becomes broad and weak in Form-H. Polymorphic phenomena are frequently found in square-planar platinum complexes due to the diversity in molecular arrangement achieved by varying intermolecular Pt···Pt and/or π–π interactions. The lower crystallinity is indicative of aggregate formation in the solid state.[51]

3.2 Crystal structure

Numerous attempts to grow (−)-**1**-TCNQ or (+)-**1**-TCNQ crystals have been unsuccessful, however, deep-green needles of racemic crystals (−)-**1**/(+)-**1**-TCNQ can luckily be obtained through slow interfacial diffusion at 278 K in a test tube, where an MeOH solution of LiTCNQ is placed at the bottom, and acetonitrile solution containing equal amounts of (+)-**1** and (−)-**1** is placed at the top. The binary cocrystal crystallizes in the space group $P2_1/c$ of a monoclinic system with one Pt(II) complex cation and one $TCNQ^{\bullet-}$ anion in an asymmetric unit (Table 1 and Fig. 3).

Selected bond distances and angles are compiled in Table 2. For the Pt(II) complex in the adduct, the Pt–C distances are 1.989(12) and 1.912(9) Å, which are similar to those of Pt(C^N^N)(Dmpi) derivatives (1.86 to 2.09 Å).[50,51] The Pt–N bond lengths (1.917(9) and 2.100(8) Å) reside in the range of 1.88–2.14 Å. For the $TCNQ^{\bullet-}$ anion in the two-component cocrystal, the exocyclic C=C bond lengths are 1.429(17) and 1.359(18) Å, while the intracyclic C=C distances are 1.320(16) and 1.319(17) Å, which are similar to those found in analogous CT complexes involved the $TCNQ^{\bullet-}$ radical anion.[47,48,59–62] Only one exocyclic C=C bond is longer than the corresponding distance of 1.37 Å in neutral species and is comparable with the 1.44 Å indicative of a radical anion. The elongation in the exocyclic C=C bond is interpreted through the presence of negative charge. The angles are also similar to those reported for Pt(II) complexes.[50,51] The

Table 1 Crystallographic data of (−)-**1**/(+)-**1**-TCNQ

	(−)-**1**/(+)-**1**-TCNQ
Formula	$PtC_{44}H_{34}N_7$
M_r/g mol^{-1}	855.87
Crystal system	Monoclinic
Space group	$P2_1/c$
a/Å	7.809(7)
b/Å	19.125(18)
c/Å	24.66(2)
α/°	90.00
β/°	90.42
γ/°	90.00
V/$Å^{-3}$	3683(6)
Z	4
T/K	296(2)
Radiation, λ/Å	0.71073
D_{calcd}, g cm^{-3}	1.543
μ/mm^{-1}	3.851
F(000)	1700
Crystal size/mm^3	0.30 × 0.15 × 0.12
θ range/°	1.35 to 25.00
Reflections measured	20 076
Unique reflections	6495
R_{int}	0.1396
Reflections with $F^2 > 2\sigma(F^2)$	3460
Number of parameters	474
Goodness-of-fit on F^2	1.082
R_1 [$F^2 > 2\sigma(F^2)$]	0.1037
wR_2 (all data)	0.2525
$\Delta\rho_{max}$, $\Delta\rho_{min}$/e $Å^{-3}$	1.501, −1.476
refine_ls_shift/su_max	0.000
refine_ls_shift/su_mean	0.000

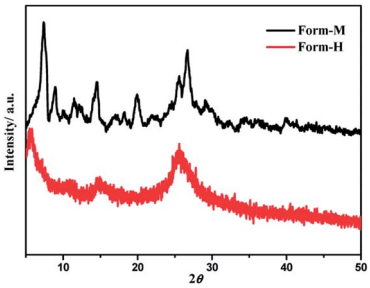

Fig. 2 Solid-state absorption spectra of Form-M and Form-H.

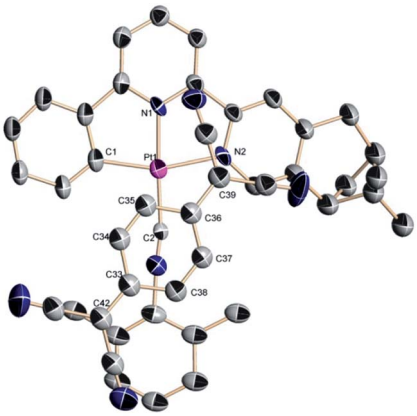

Fig. 3 X-ray crystal structure of a (−)-**1**/(+)-**1**-TCNQ cocrystal. H atoms are omitted for clarity.

Open Access Article. Published on 16 March 2018. Downloaded on 5/9/2026 5:12:19 PM.
This article is licensed under a Creative Commons Attribution-NonCommercial 3.0 Unported Licence.

Table 2 The structural parameters of (−)-**1**/(+)-**1**-TCNQ determined *via* X-ray single crystal diffraction

Bond length		Bond angle	
Pt1–C1	1.989(12)	C1–Pt1–C2	99.7(4)
Pt1–C2	1.912(9)	C1–Pt1–N1	82.9(4)
Pt1–N1	1.917(9)	C1–Pt1–N2	161.4(4)
Pt1–N2	2.100(8)	C2–Pt1–N1	177.2(4)
C36–C39	1.429(17)	C2–Pt1–N2	98.8(4)
C34–C35	1.320(16)	N1–Pt1–N2	78.7(4)
C37–C38	1.319(17)		
C33–C42	1.359(18)		

interchelate C1–Pt1–N2 angle (161.4(4)°) deviates substantially from 180° as a result of terdentate-bonding ring strain. And the N1–Pt1–C2 angle (177.2(4)°) is close to linearity. In our previous studies, the moiety of 2,6-dimethylphenyl isocyanide is almost coplanar with the Pt(C^N^N) unit,[50,51] however, a larger torsion angle between these two planes is exhibited in the (−)-**1**/(+)-**1**-TCNQ cocrystal (Fig. S4†).

A crystal packing diagram of the cocrystal along the *a*-axis is presented in Fig. 4. The $TCNQ^{\bullet-}$ anion and Pt(II) complex cation form one-dimensional chains in a 1 : 1 pattern, adopting a face-to-face arrangement. The interplanar separations (Pt–π) of alternating (−)-**1** cations and $TCNQ^{\bullet-}$ moieties are 3.637(3) Å and 4.263(4) Å. According to previous studies, interplanar distances between donor and acceptor molecules within 3.75 Å are in the range reported for π–π, d–π, and electrostatic donor–acceptor interactions, therefore it can be inferred that weak charge-transfer (donor–acceptor) interactions are present in the cocrystal.[47,48,59,60] Moreover, in the *bc* plane, neighboring columns of (−)-**1**-TCNQ/(+)-**1**-TCNQ CT adducts are stacked alternately (Fig. S5†).

3.3 Absorption and emission properties

In the above studies, (−)-**1**/(+)-**1** cations and $TCNQ^{\bullet-}$ anions can form CT adducts, as evidenced by the crystal structure; also, the powders with different colors obtained in MeOH and H_2O suggest that the solvent is essential in inducing polymorphism with variable CT properties.[63,64] The solvent-tuned spectroscopic variances in (−)-**1**-TCNQ will be investigated in the following discussion. The parent compound (−)-**1** is reported to show characteristic intraligand (IL) transitions ($\varepsilon > 10^4$ L mol^{-1} cm^{-1}) in the region of 200–310 nm, and metal-to-ligand charge transfer (MLCT) mixed with ligand-to-ligand charge transfer (LLCT) transitions ($\varepsilon > 10^3$ L mol^{-1} cm^{-1}) in the region of 330–450 nm in MeOH solution (Fig. 5).[50] And the $TCNQ^{\bullet-}$ anion presents a series of pronounced absorption bands in the low-energy region (600–900 nm) and a peak centered at *ca.* 418 nm in the visible range, which is in line with the reported electronic excitation spectrum of the $TCNQ^{\bullet-}$ anion, and agrees well with previous interpretations of the calculated excitation energies.[47,48,65,66]

During a titration experiment, LiTCNQ at various ratios is added to a MeOH solution of (−)-**1** (Fig. 5). It can be observed that no new absorption bands appear. Moreover, when the mole ratio reaches 1 : 1, the low-energy absorptions ranging from 600 to 900 nm with regards to the $TCNQ^{\bullet-}$ anion and the high-energy absorptions ranging from 220 to 350 nm mainly relating to parent compound (−)-**1** are almost identical to the individual absorption spectra of the Pt(II) complex cation and $TCNQ^{\bullet-}$ anion. Therefore, any bound complex between the parent compound (−)-**1** cation and $TCNQ^{\bullet-}$ anion has not been formed in MeOH solution, and they are dissociated and hardly perturb the electronic structures of each other.

Our previous studies showed that (−)-**1** and (+)-**1** could aggregate into one dimensional supramolecular structures through Pt···Pt, π–π, and hydrophobic–hydrophobic interactions in aqueous solution.[50] Interestingly, when LiTCNQ is added to a H_2O solution of (−)-**1**, three new bands at 623, 756 and 860 nm emerge and are strengthened progressively with the incremental addition of LiTCNQ (Fig. 6). In addition, the absorption band at 335 nm of the parent compound (−)-**1** is red-shifted to 357 nm upon introducing an equal proportion of $TCNQ^{\bullet-}$ anion. Compared to the individual absorption spectra of (−)-**1** and $TCNQ^{\bullet-}$ in H_2O, the spectrum of the (−)-**1**-TCNQ adduct is not a mixture of the UV-vis spectra of each component. For the lowest energy absorption, the peak at 830 nm from the $TCNQ^{\bullet-}$ anion is red-shifted to 860 nm and, simultaneously, the extinction coefficient is attenuated. CT adducts between the parent compound (−)-**1** cation and $TCNQ^{\bullet-}$ anion in H_2O have been generated through effective intermolecular interactions, *e.g.* Pt–π and π–π, and then the electronic structures are significantly perturbed by each other, leading to different transitions and UV-vis spectra.[47,48] According to computational studies in the literature, the HOMO is localized on the chiral Pt(II) compound (−)-**1**, while the LUMO is distributed on the

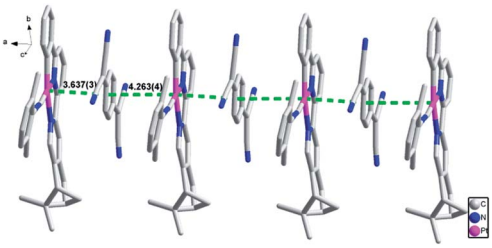

Fig. 4 A crystal packing diagram of (−)-**1**/(+)-**1**-TCNQ along the *a*-axis with green dashed lines indicating Pt···π interactions.

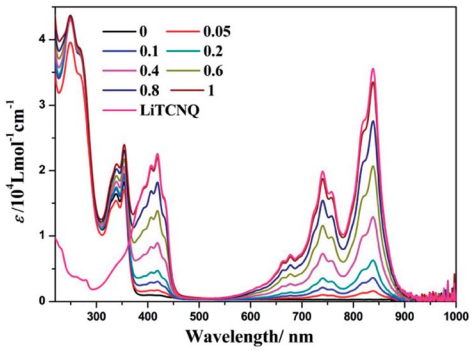

Fig. 5 UV-vis spectra of LiTCNQ and the complex (−)-**1** after the addition of LiTCNQ at various ratios in MeOH.

Open Access Article. Published on 16 March 2018. Downloaded on 5/9/2026 5:12:19 PM.
This article is licensed under a Creative Commons Attribution-NonCommercial 3.0 Unported Licence.

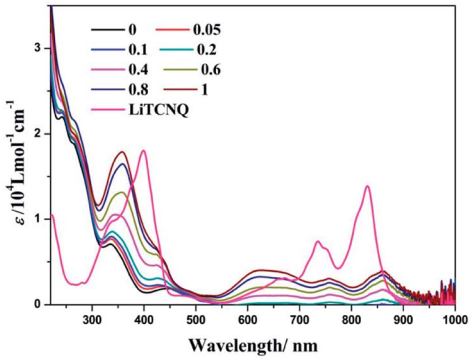

Fig. 6 UV-vis spectra of LiTCNQ and the complex (−)-**1** after the addition of LiTCNQ at various ratios in H_2O.

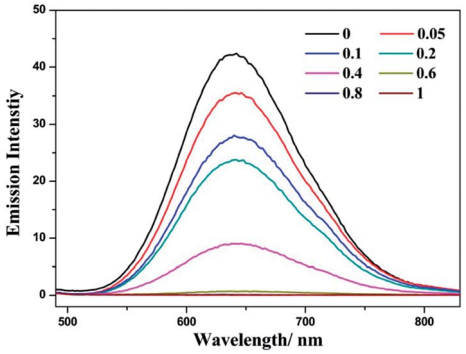

Fig. 8 Emission spectra of complex (−)-**1** after the addition of LiTCNQ at various ratios in H_2O.

$TCNQ^{\bullet-}$ anion, so the CT band observed at 860 nm is tentatively assigned to a charge transfer transition from the Pt(II) complex cation to the $TCNQ^{\bullet-}$ anion.[65,66]

Complex (−)-**1** is emissive in both MeOH and H_2O solution. During the addition of LiTCNQ, different attenuation rates of emission intensity have been observed. In MeOH, the emission intensity is weakened gradually with the incremental addition of LiTCNQ, and the emission can be detected unambiguously even when the mole ratio attains a value of 1 : 1 (Fig. 7). However, the emission intensity is attenuated sharply in H_2O solution, and luminescence can be neglected when the mole ratio is 0.6 (Fig. 8). This result is consistent with the absorption spectra, where the (−)-**1** cation and $TCNQ^{\bullet-}$ anion are almost disassociated in MeOH and strongly interact with each other in H_2O. As a consequence, the emission decay in MeOH is attributed to weak energy transfer between the (−)-**1** cation and $TCNQ^{\bullet-}$ anion,[67] while luminescence quenching in H_2O is mainly due to strong charge transfer and energy transfer.[47,48]

The solvent-induced difference between forming CT adducts in MeOH and H_2O has been further evidenced using resonance light scattering (RLS) spectra. In MeOH solution, the RLS intensity is not enhanced distinctly upon the addition of LiTCNQ (Fig. 9). To the contrary, the intensity of the RLS signal over the range of 300 to 600 nm is significantly strengthened upon adding LiTCNQ in H_2O solution (Fig. 10), and shows a 10-fold increase when the mole ratio is 1 : 1, implying the formation of CT adducts in solution and therefore that the chromophores are strongly coupled.[50,68–70]

3.4 Electronic circular dichroism (ECD) spectra

The chiral environment of (−)-**1** after the addition of LiTCNQ has been explored in MeOH and H_2O solutions through recording the electronic circular dichroism (ECD) spectra. Upon the introduction of LiTCNQ in MeOH solution, the chiral signal of (−)-**1** remains unchanged, showing positive Cotton effects at 240, 284 and 346 nm and negative Cotton effects at 303 nm (Fig. 11). In H_2O solution, molecules of (−)-**1** and (+)-**1** could form helical packing structures and present enhanced chiral signals (positive Cotton effects: 250, 300, 370 and 480 nm; negative Cotton effects: 320 and 420 nm). After adding LiTCNQ to a H_2O solution of (−)-**1**, significant variance in Cotton effects can be observed, which suggests the emergence of chiral transfer in H_2O solution (Fig. 12).[71,72] The positive Cotton effects at 300 and 370 grow progressively more intense. When the mole ratio reaches 1 : 1, the negative peak at 320 nm and the positive peak at 480 nm vanish, and the negative Cotton effect at 420 nm is red-shifted to 433 nm. Furthermore, a new positive Cotton effect at 600 nm can be perceived (Fig. 12). The difference in ECD spectra is in accordance with the solvent-induced absorption properties, as shown in Fig. 5 and 6.

To check whether any artifacts have been introduced into the spectra, the ECD signals of enantiomers (+)-**1** and (+)-**1**-TCNQ

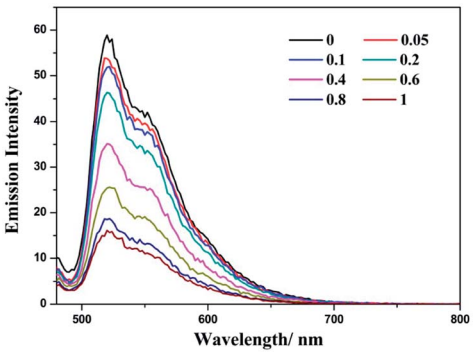

Fig. 7 Emission spectra of complex (−)-**1** after the addition of LiTCNQ at various ratios in MeOH.

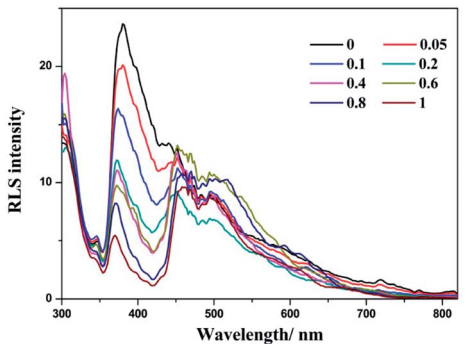

Fig. 9 RLS spectra of (−)-**1** after the addition of LiTCNQ at various ratios in MeOH.

Open Access Article. Published on 16 March 2018. Downloaded on 5/9/2026 5:12:19 PM.
This article is licensed under a Creative Commons Attribution-NonCommercial 3.0 Unported Licence.

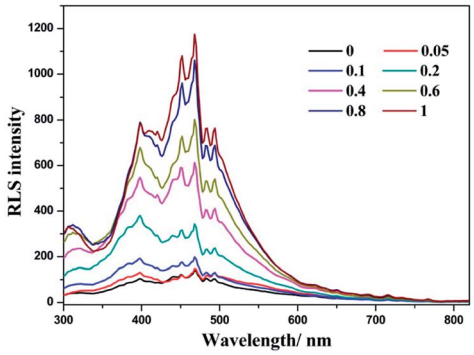

Fig. 10 RLS spectra of (−)-**1** after the addition of LiTCNQ at various ratios in H_2O.

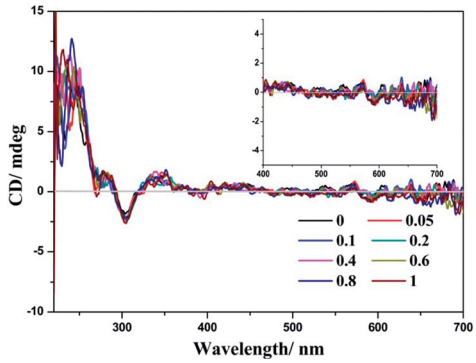

Fig. 11 ECD spectra of complex (−)-**1** after the addition of LiTCNQ at various ratios in MeOH.

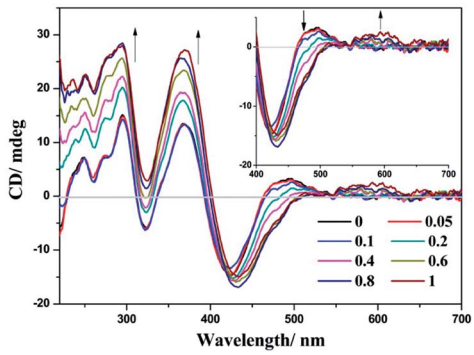

Fig. 12 ECD spectra of complex (−)-**1** after the addition of LiTCNQ at various ratios in H_2O.

have been measured under the same conditions, and perfect mirror images of each other are exhibited (Fig. S6 and S7†). Generally, Pt(II) complexes undergo chiral amplification and chiral transfer through self-assembly into chiral supramolecular aggregates or through varying the configuration around the metal center.[49–54] Several examples show that adding chiral acceptors or donors can also amplify the chiral signal.[73] The (−)-**1** cation and $TCNQ^{\bullet-}$ anion can form CT adducts in H_2O *via* Pt–π, π–π and electrostatic interactions, and the presence of the organic acceptor $TCNQ^{\bullet-}$ anion would influence the geometry, perturb the electronic structure and alter the chiral environment, owing to strong intermolecular interactions. Therefore, charge transfer and chiral transfer phenomena occur in H_2O solution, while the (−)-**1** cation and $TCNQ^{\bullet-}$ anion are not likely to significantly perturb each other in MeOH solution.

4. Conclusions

We succeeded in the preparation and characterization of a new pair of adducts involving one chiral Pt(II) complex cation and one $TCNQ^{\bullet-}$ anion. The charge-transfer properties as well as the chiral signals of the adducts can be tuned *via* the solvent. In MeOH, the Pt(II) complex cation and $TCNQ^{\bullet-}$ anion are non-interacting, and the UV-vis spectrum of the (−)-**1**-TCNQ adduct is just a mixture of individual absorption bands. In addition, the chiral signals in MeOH solution are completely derived from the chiral Pt(II) complex cation. However, CT aggregates between the parent compound (−)-**1** cation and $TCNQ^{\bullet-}$ anion have been formed in H_2O solution through effective intermolecular interactions (Pt–π, π–π and electrostatic attraction), and their electronic structures and chiral environments have been significantly influenced, leading to different transitions in UV-vis spectra and diverse Cotton effects in ECD spectra. Furthermore, the exploration of the emission and RLS spectra also affirms the formation of strongly interacting CT adducts in H_2O solution. The results can provide some guidance for fabricating semiconductor devices and solar cells based on charge transfer salts.

Conflicts of interest

There are no conflicts to declare.

Acknowledgements

This work is supported by the National Natural Science Foundation of China (Grant No. 21601043), and the Natural Science Foundation of Hainan Province (20162026, 217100, 217101, ZDYF2017011 and 2017CXTD007).

Notes and references

1 X. Wang and Z. Guo, *Chem. Soc. Rev.*, 2013, **42**, 202–224.
2 V. W.-W. Yam, V. K.-M. Au and S. Y.-L. Leung, *Chem. Rev.*, 2015, **115**, 7589–7728.
3 J. R. Brandt, X. Wang, Y. Yang, A. J. Campbell and M. J. Fuchter, *J. Am. Chem. Soc.*, 2016, **138**, 9743–9746.
4 K. T. Ly, R.-W. Chen-Cheng, H.-W. Lin, Y.-J. Shiau, S.-H. Liu, P.-T. Chou, C.-S. Tsao, Y.-C. Huang and Y. Chi, *Nat. Photonics*, 2017, **11**, 63–68.
5 T. Fleetham, G. Li and J. Li, *Adv. Mater.*, 2017, **29**, 1601861.
6 S. Carrara, A. Aliprandi, C. F. Hogan and L. De Cola, *J. Am. Chem. Soc.*, 2017, **139**, 14605–14610.
7 Y. Sagara and T. Kato, *Nat. Chem.*, 2009, **1**, 605–610.
8 O. S. Wenger, *Chem. Rev.*, 2013, **113**, 3686–3733.

Open Access Article. Published on 16 March 2018. Downloaded on 5/9/2026 5:12:19 PM.
This article is licensed under a Creative Commons Attribution-NonCommercial 3.0 Unported Licence.

9 X. Zhang, Z. Chi, Y. Zhang, S. Liu and J. Xu, *J. Mater. Chem. C*, 2013, **1**, 3376–3390.
10 A. Aliprandi, D. Genovese, M. Mauro and L. De Cola, *Chem. Lett.*, 2015, **44**, 1152–1169.
11 Y. Sagara, S. Yamane, M. Mitani, C. Weder and T. Kato, *Adv. Mater.*, 2016, **28**, 1073–1095.
12 J. Moussa, K. M.-C. Wong, X. F. L. Goff, M. N. Rager, C. K.-M. Chan, V. W.-W. Yam and H. Amouri, *Organometallics*, 2013, **32**, 4985–4992.
13 J. Moussa, K. Haddouche, L.-M. Chamoreau, H. Amouri and J. A. G. Williams, *Dalton Trans.*, 2016, **45**, 12644–12648.
14 H. Sesolis, C. K.-M. Chan, G. Gontard, H. L.-K. Fu, V. W.-W. Yam and H. Amouri, *Organometallics*, 2017, **36**, 4794–4801.
15 W. Lu, Y. Chen, V. A. L. Roy, S. S.-Y. Chui and C.-M. Che, *Angew. Chem., Int. Ed.*, 2009, **48**, 7621–7625.
16 C.-H. Wong, C. Po, S. Y.-L. Leung, A. K.-W. Chan, S. Yang, B. Zhu, X. Cui and V. W.-W. Yam, *J. Am. Chem. Soc.*, 2018, **140**, 657–666.
17 J. Ni, X. Zhang, Y.-H. Wu, L.-Y. Zhang and Z.-N. Chen, *Chem.–Eur. J.*, 2011, **17**, 1171–1183.
18 M. J. Bryant, J. M. Skelton, L. E. Hatcher, C. Stubbs, E. Madrid, A. R. Pallipurath, L. H. Thomas, C. H. Woodall, J. Christensen, S. Fuertes, T. P. Robinson, C. M. Beavers, S. J. Teat, M. R. Warren, F. Pradaux-Caggiano, A. Walsh, F. Marken, D. R. Carbery, S. C. Parker, N. B. McKeown, R. Malpass-Evans, M. Carta and P. R. Raithby, *Nat. Commun.*, 2017, **8**, 1800.
19 A. Kobayashi, N. Yamamoto, Y. Shigeta, M. Yoshida and M. Kato, *Dalton Trans.*, 2018, **47**, 1548–1556.
20 M. Krikorian, S. Liu and T. M. Swager, *J. Am. Chem. Soc.*, 2014, **136**, 2952–2955.
21 S. S. Pasha, P. Alam, A. Sarmah, R. K. Roy and I. R. Laskar, *RSC Adv.*, 2016, **6**, 87791–87795.
22 A. F. Henwood, J. Webster, D. Cordes, A. M. Z. Slawin, D. Jacquemin and E. Zysman-Colman, *RSC Adv.*, 2017, **7**, 25566–25574.
23 M. H.-Y. Chan, M. Ng, S. Y.-L. Leung, W. H. Lam and V. W.-W. Yam, *J. Am. Chem. Soc.*, 2017, **139**, 8639–8645.
24 K. M. C. Wong and V. W. W. Yam, *Acc. Chem. Res.*, 2011, **44**, 424–434.
25 T. Ikeda, M. Takayama, J. Kumar, T. Kawai and T. Haino, *Dalton Trans.*, 2015, **44**, 13156–13162.
26 H. L.-K. Fu, C. Po, H. He, S. Y.-L. Leung, K. S. Wong and V. W.-W. Yam, *Chem.–Eur. J.*, 2016, **22**, 1–12.
27 S. Tanaka, K. Sato, K. Ichida, T. Abe, T. Tsubomura, T. Suzuki and K. Shinozaki, *Chem.–Asian J.*, 2016, **11**, 265–273.
28 A. Aliprandi, C. M. Croisetu, M. Mauro and L. De Cola, *Chem.–Eur. J.*, 2017, **23**, 1–6.
29 T. Ikeda, K. Hirano and T. Haino, *Mater. Chem. Front.*, 2018, **2**, 468–474.
30 H. Sesolis, J. Dubarle-Offner, C. K. M. Chan, E. Puig, G. Gontard, P. Winter, A. L. Cooksy, V. W. W. Yam and H. Amouri, *Chem.–Eur. J.*, 2016, **22**, 8032–8037.
31 M. Liu, L. Zhang and T. Wang, *Chem. Rev.*, 2015, **115**, 7304–7397.
32 J.-F. Mei, X.-Y. Jia, J.-C. Lai, Y. Sun, C.-H. Li, J.-H. Wu, Y. Cao, X.-Z. You and Z. Bao, *Macromol. Rapid Commun.*, 2016, **37**, 1667–1675.
33 A. Aliprandi, M. Mauro and L. De Cola, *Nat. Chem.*, 2016, **8**, 10–15.
34 L. Ravotto and P. Ceroni, *Coord. Chem. Rev.*, 2017, **346**, 62–76.
35 Y. Krupskaya, M. Gibertini, N. Marzari and A. F. Morpurgo, *Adv. Mater.*, 2015, **27**, 2453–2458.
36 K. Kang, S. Watanabe, K. Broch, A. Sepe, A. Brown, I. Nasrallah, M. Nikolka, Z. Fei, M. Heeney, D. Matsumoto, K. Marumoto, H. Tanaka, S.-i. Kuroda and H. Sirringhaus, *Nat. Mater.*, 2016, **15**, 896–902.
37 X. Zhang, Z.-X. Wang, H. Xie, M.-X. Li, T. J. Woods and K. R. Dunbar, *Chem. Sci.*, 2016, **7**, 1569–1574.
38 L. Ballester, A. M. Gil, A. Gutiérrez, M. F. Perpiñán, M. T. Azcondo, A. E. Sánchez, C. Marzin, G. Tarrago and C. Bellitto, *Chem.–Eur. J.*, 2002, **8**, 2539–2548.
39 X. Qu, J. Lu, C. Zhao, J. F. Boas, B. Moubaraki, K. S. Murray, A. Siriwardana, A. M. Bond and L. L. Martin, *Angew. Chem.*, 2011, **123**, 1627–1630.
40 R. Ramanathan, S. Walia, A. E. Kandjani, S. Balendran, M. Mohammadtaheri, S. K.Bhargava, K. Kalantar-zadeh and V. Bansal, *Langmuir*, 2015, **31**, 1581–1587.
41 L. Sutton, B. F. Abrahams, D. M. D'Alessandro, T. A. Hudson, R. Robson and P. M. Usov, *CrystEngComm*, 2016, **18**, 8906–8914.
42 J. Kim, A. Silakov, H. P. Yennawar and B. J. Lear, *Inorg. Chem.*, 2015, **54**, 6072–6074.
43 A. P. O'Mullane, N. Fay, A. Nafady and A. M. Bond, *J. Am. Chem. Soc.*, 2007, **129**, 2066–2073.
44 A. Nagai and Y. Okabeb, *Chem. Commun.*, 2014, **50**, 10052–10054.
45 J. Jalkh, Y. R. Leroux, A. Vacher, D. Lorcy, P. Hapiot and C. Lagrost, *J. Phys. Chem. C*, 2016, **120**, 28021–28030.
46 C. Wang, N. Wu, D. L. Jacobs, M. Xu, X. Yang and L. Zang, *Chem. Commun.*, 2017, **53**, 1132–1135.
47 W.-H. Chen, E. W. Reinheimer, K. R. Dunbar and M. A. Omary, *Inorg. Chem.*, 2006, **45**, 2770–2772.
48 C. rowning, J. M. Hudson, E. W. Reinheimer, F.-L. Kuo, R. N. McDougald Jr, H. Rabaâ, H. Pan, J. Bacsa, X. Wang, K. R. Dunbar, N. D. Shepherd and M. A. Omary, *J. Am. Chem. Soc.*, 2014, **136**, 16185–16200.
49 X.-P. Zhang, T. Wu, J. Liu, J.-X. Zhang, C.-H. Li and X.-Z. You, *J. Mater. Chem. C*, 2014, **2**, 184–194.
50 X.-P. Zhang, V. Y. Chang, J. Liu, X.-L. Yang, W. Huang, Y. Li, C.-H. Li, G. Muller and X.-Z. You, *Inorg. Chem.*, 2015, **54**, 143–152.
51 X.-P. Zhang, J.-F. Mei, J.-C. Lai, C.-H. Li and X.-Z. You, *J. Mater. Chem. C*, 2015, **3**, 2350–2357.
52 X.-P. Zhang, L. Zhu, X. Wang, Z. Shi and Q. Lin, *Inorg. Chim. Acta*, 2016, **442**, 56–63.
53 X.-P. Zhang, F.-Q. Liu, J.-C. Lai, C.-H. Li, A.-M. Li and X.-Z. You, *New J. Chem.*, 2016, **40**, 2628–2636.
54 X.-P. Zhang, D.-S. Zhang, X.-W. Qi, L.-H. Zhu, X.-H. Wang, W. Sun, Z.-F. Shi and Q. Lin, *Inorg. Chim. Acta*, 2017, **467**, 99–105.

 This journal is © The Royal Society of Chemistry 2018

Open Access Article. Published on 16 March 2018. Downloaded on 5/9/2026 5:12:19 PM.
This article is licensed under a Creative Commons Attribution-NonCommercial 3.0 Unported Licence.

55 *SAINT-Plus, version 6.02, Bruker Analytical X-ray System*, Madison, WI, 1999.
56 G. M. Sheldrick, *SADABS, an empirical absorption correction program, Bruker Analytical X-ray Systems*, Madison, WI, 1996.
57 G. M. Sheldrick, *Acta Crystallogr., Sect. A: Cryst. Phys., Diffr., Theor. Gen. Crystallogr.*, 2008, **64**, 112.
58 J.-Y. Zhang, L.-J. Su, Q.-J. Guo and J. Tao, *Inorg. Chem. Commun.*, 2017, **82**, 39–43.
59 B. W. Smucker, J. M. Hudson, M. A. Omary and K. R. Dunbar, *Inorg. Chem.*, 2003, **42**, 4714–4723.
60 S. Shibahara, H. Kitagawa, Y. Ozawa, K. Toriumi, T. Kubo and K. Nakasuji, *Inorg. Chem.*, 2007, **46**, 1162–1170.
61 S. Yang, F. Pop, C. Melan, A. C. Brooks, L. Martin, P. Horton, P. Auban-Senzier, G. L. J. A. Rikken, N. Avarvari and J. D. Wallis, *CrystEngComm*, 2014, **16**, 3906–3916.
62 M. A. Dobrowolski, G. Garbarino, M. Mezouar, A. Ciesielski and M. K. Cyrański, *CrystEngComm*, 2014, **16**, 415–429.
63 P. Hu, L. Ma, K. J. Tan, H. Jiang, F. Wei, C. Yu, K. P. Goetz, O. D. Jurchescu, L. E. McNeil, G. G. Gurzadyan and C. Kloc, *Cryst. Growth Des.*, 2014, **14**, 6376–6382.
64 H. Sun, M. Wang, X. Wei, R. Zhang, S. Wang, A. Khan, R. Usman, Q. Feng, M. Du, F. Yu, W. Zhang and C. Xu, *Cryst. Growth Des.*, 2015, **15**, 4032–4038.
65 T. R. Cundari, B. Chilukuri, J. M. Hudson, C. Minot, M. A. Omary and H. Rabaâ, *Organometallics*, 2010, **29**, 795–800.
66 H. Rabaâ, S. Taubert and D. Sundholm, *J. Phys. Chem. A*, 2013, **117**, 12363–12373.
67 P. Du and R. Eisenberg, *Chem. Sci.*, 2010, **1**, 502–506.
68 R. F. Pasternack and P. J. Collings, *Science*, 1995, **269**, 935–939.
69 H. Pan, X. Tao, C. Mao, J.-J. Zhu and F. Liang, *Talanta*, 2007, **71**, 276–281.
70 S. Y.-L. Leung and V. W.-W. Yam, *Chem. Sci.*, 2013, **4**, 4228–4234.
71 J. Crassous, *Chem. Soc. Rev.*, 2009, **38**, 830–845.
72 M. Liu, L. Zhang and T. Wang, *Chem. Rev.*, 2015, **115**, 7304–7397.
73 J. Han, P. Duan, X. Li and M. Liu, *J. Am. Chem. Soc.*, 2017, **139**, 9783–9786.